Parameter exploration of optically trapped liquid aerosols

D. R. Burnham,[1,2,*] P. J. Reece,[1,†] and D. McGloin[2]
[1]*SUPA, School of Physics and Astronomy, University of St. Andrews, North Haugh, Fife KY16 9SS, United Kingdom*
[2]*SUPA, Electronic Engineering and Physics Division, University of Dundee, Nethergate, Dundee DD1 4HN, United Kingdom*
(Received 28 June 2010; published 17 November 2010)

When studying the motion of optically trapped particles on the microsecond time scale, in low-viscosity media such as air, inertia cannot be neglected. Resolution of unusual and interesting behavior not seen in colloidal trapping experiments is possible. In an attempt to explain the phenomena we use power-spectral methods to perform a parameter study of the Brownian motion of optically trapped liquid aerosol droplets concentrated around the critically damped regime. We present evidence that the system is suitably described by a simple harmonic oscillator model which must include a description of Faxén's correction, but not necessarily frequency dependent hydrodynamic corrections to Stokes' law. We also provide results describing how the system behaves under several variables and discuss the difficulty in decoupling the parameters responsible for the observed behavior. We show that due to the relatively low dynamic viscosity and high trap stiffness, it is easy to transfer between over- and underdamped motion by experimentally altering either trap stiffness or damping. Our results suggest stable aerosol trapping may be achieved in underdamped conditions, but the onset of deleterious optical forces at high trapping powers prevents the probing of the upper stability limits due to Brownian motion.

DOI: 10.1103/PhysRevE.82.051123 PACS number(s): 05.40.Jc, 42.50.Wk, 82.70.Rr

I. INTRODUCTION

In a number of recent publications our group [1–3] has presented an experimental system, based on the optical trapping of aerosols, for studying Brownian dynamics in both over- and underdamped conditions. With this unique perspective, we are able to investigate the emergence of phenomena such as oscillatory motions due to the influence of inertial forces. This is a significant departure from traditional optical trapping experiments, which are performed under conditions of heavy viscous damping [4].

When understood [5], Brownian motion can be used in conjunction with optical detection to determine the size of microscopic colloidal suspensions [6,7] or to measure Avogadro's number [8]. Recently it has allowed optical traps to provide a powerful tool in diverse research fields capable of acting as a force transducer for molecular biology [9], viscometry [10], microscopy [11], and fundamental physics [12]. These applications often use the power spectrum method [13] to detect position [14], measure forces [15], or investigate colloidal dynamics [16] and rely on the study of overdamped systems [17].

The investigation of overdamped systems via optical trapping has produced classic experiments with important physical results including tests of Kramer's theory [18], measurements of critical Casimir forces [12] and demonstrations of fluctuation theorems [19]. The various optical potentials created through optical manipulation have, for example, been used to investigate colloidal crystals [20,21], with particle dynamics providing analogies in thermal ratchets [22] and freezing [23].

All experiments with optical tweezers in a liquid environment behave as overdamped oscillators, but there have been discussions that underdamped motions are observed [24] and comments that this should not be possible [17,25]. What is true is that studies of nonoverdamped systems are rare [2,26]. However, this looks set to change with a recent resurgence in the original airborne particle experiments of Ashkin [3,27–29]. The main applications of such experiments are in aerosol science with most studies to date investigating the chemistry of liquid droplets in gas phase environments [30,31], but they also offer more esoteric possibilities with opportunities to study quantum mechanical effects linked to Brownian motion [32]. Due to the importance of inertia in such systems they provide a drastically different damping environment and hence experimental possibilities.

When comparing airborne to aqueous trapping, several phenomena may be observed that would be considered unusual. Varying trapping power alters the axial equilibrium position of droplets resulting in "power gradients" [33] with further increases in power causing their loss. Given a polydisperse nebulised sample, the initial power used to capture a droplet has pronounced size selectivity [34,35] and once trapped, the droplet can undergo vertical oscillations at frequencies of $\sim 0.1-10$ Hz.

This parameter study of the 'mechanical' forces in airborne optical traps was conducted in an attempt to explain various phenomena, but also proves useful in developing a deeper understanding of aerosol trapping. A limited exploration has previously been carried out showing a trapped droplet can behave in either an over- or underdamped manner and that parametric resonance is easily excited [2]. In addition we have observed underdamped behavior in two particle systems [26]. This paper investigates the transition from over- to underdamped in more detail, exploring the parameter space by discussing dependence on laser power, droplet size, and depth into the sample at which the droplet is trapped. We show the system can be described by a simple harmonic

*Present address: Department of Chemistry, University of Washington, Box 351700, Seattle, WA 98195-1700, USA.
†Also at School of Physics, The University of New South Wales, Sydney, NSW 2052, Australia.

oscillator model by including appropriate corrections. We also test the hypothesis that droplets are lost from their traps as the power is increased because they cross into the underdamped regime.

Several methods have been presented to characterize the Brownian dynamics of a trapped object, all relying on position measurement, including the drag force method, the equipartition method, the step response method, autocorrelation, and the power spectrum method [36]. Position-sensitive detectors, video tracking or quadrant photodiodes (QPDs) are often used to detect particle position, each with their own speed and precision advantages and disadvantages [37,38]. Here we employ a QPD due to the high bandwidth and the power spectrum method, which is considered the most reliable [39], to characterize the Brownian motion of droplets within optical traps. The autocorrelation of a single particle is also feasible but can provide poor results in noisy systems. The power spectrum method decomposes the motion into frequency components so any noise can be easily dealt with. Although we are mainly concerned with observing the dynamics of trapped aerosols, it is feasible to use this method to measure precise forces and position. Normally the method allows calculation of trap stiffness with prior knowledge of the viscosity of the surrounding medium and the particle radius [36], but it will be shown here that in air only the radius is needed.

First we will discuss the theory used to describe our experimental system along with any subtle corrections that may need to be considered and what the magnitude of their effect would be. We will then describe our experimental apparatus and procedures which differ slightly from optical trapping in aqueous media. We will also present evidence that supports that our system can be described by a simple harmonic oscillator model with certain corrections included. Finally we will try to determine the cause of the unusual behavior partly by studying how trapped droplets behave near the critically damped regime.

II. THEORY

Throughout this work we assume that particle velocity is well below the speed of sound and the propagations of interactions in the fluid are instantaneous, hence the fluid, air, is treated as incompressible [40]. An optically trapped particle is treated as residing in a harmonic potential well experiencing a Hookean restoring force when displaced through Brownian stochastic forces. The characteristic time for such a particle to lose energy through friction is a balance between inertial and viscous forces, $t_{inert}=m/\gamma_0$ [41], where m is the particle mass and γ_0 is the viscous drag. For the smallest droplet studied here this time is longer than our experimental resolution so inertia must not be neglected as is usual for studies in liquid media. The Langevin equation describing the motion of a liquid aerosol of radius R, mass m, optically trapped in a fluid of temperature T, kinematic viscosity ν, and density ρ_{fluid}, with stiffness κ is [42]

$$\ddot{x}(t)+\Gamma\dot{x}(t)+\Omega^2 x(t)=\Lambda\zeta(t), \tag{1}$$

where $\Omega=\sqrt{(\kappa/m)}$ is the natural angular frequency of the droplet position fluctuations, $\Gamma=6\pi\eta R/mC_c$ is the viscous damping of the medium due to a dynamic viscoscity $\eta=\rho_{fluid}\nu$, $\Lambda=(2k_BT\Gamma/m)^{1/2}$ [43,44] is the Brownian stochastic force where k_B is the Boltzmann constant, and for all t and t', $\langle\zeta(t)\rangle=0$ and $\langle\zeta(t)\zeta(t')\rangle=\delta(t-t')$. Stokes' Law is corrected for finite Knudsen number effects by including the empirical slip correction factor, C_c, with a 5.5–1.6 % reduction in drag for 3–10 μm diameter droplets, respectively [45]. Fourier transforming Eq. (1) and finding the expectation value we can decompose the motion into frequency components and find the power spectrum of position fluctuations to be

$$S_x^{inertia}(\omega)=\frac{2k_BT}{\kappa}\frac{\Omega^2\Gamma}{(\omega^2-\Omega^2)^2+\omega^2\Gamma^2}, \tag{2}$$

where ω is the angular frequency. This spectrum has a characteristic high frequency tail with ω^{-4} gradient and a plateau value at low frequencies equal to $2k_BT\Gamma/\kappa\Omega^2$. As inertia is included, there is an additional limiting case compared to overdamped oscillators at the point of inflection equal to $2k_BT/\kappa\Gamma$. We define the ratio of damping coefficient to natural frequency as the "damping ratio," Γ/Ω. For overdamped systems this is always greater than unity, as is found for colloidal systems where it is usually greater than ten. In such cases the first angular frequency term in the denominator can be neglected with respect to Ω, to give the usual power spectrum for overdamped optical traps [2]. When trapping in air, the system has the potential to become underdamped and hence $\Gamma/\Omega<1$.

The above Langevin equation assumes the motion occurs in bulk fluid media with uniform velocity, far away from other objects and surfaces, so Stokes' law is only corrected for finite Knudsen number. However, in reality the objects here are undergoing linear harmonic motion within significant proximity ($\leq 10R$) of a coverslip so it is inappropriate to assume Stokes' law still applies. Studying this problem, it is seen there are two significant corrections that may need to be applied to the "in bulk" theory.

First, the object is undergoing linear harmonic motion and so a more complex, frequency-dependent friction must be considered, which was shown by Stokes to be [40,41,46]

$$F_{friction}=-\gamma_0\left(1+\sqrt{\frac{R^2\omega}{2\nu}}\right)\dot{x}-\frac{2}{3}\pi\rho_{fluid}R^3\left(1+\frac{9}{2}\sqrt{\frac{2\nu}{R^2\omega}}\right)\ddot{x}. \tag{3}$$

The first term comprises the familiar Stokes' drag plus a frequency-dependent correction. The second term arises from the inertia created by any fluid entrained due to the past motion of the particle. This hydrodynamic correction is often neglected [2,9,24,47,48], at times with good cause, but needs to be applied when requiring precision >10% [41]. Here we will try to justify our exclusion of such terms in a little detail.

Using Eq. (3) and following Berg-Sørensen and Flyvbjerg [41], we derive the hydrodynamically correct power spectrum in angular frequency to be

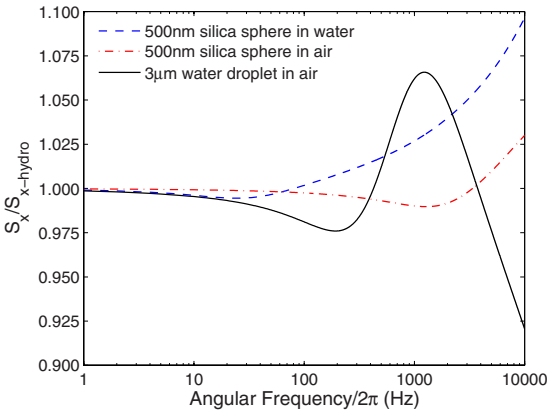

FIG. 1. (Color online) Theoretical plot of $S_x/S_{x-hydro}$ as a function of angular frequency. For a given particle radius the hydrodynamic correction is smaller in air (red dot dashed) than in water (blue dashed), but, for the large liquid aerosols (black solid) the effect starts to become significant. Trap stiffness, $\kappa=2$ pN μm^{-1}.

$$S_{x-hydro}^{inert}(\omega) = \frac{2k_BT}{\kappa}\frac{\Omega^2\Gamma\left[1+\left(\frac{\omega}{\omega_\nu}\right)^{1/2}\right]}{\left[\Omega^2-\Gamma\left(\frac{\omega^{3/2}}{\omega_\nu^{1/2}}\right)-\frac{\omega^2\Gamma}{\omega_m}\right]^2+\left[\omega\Gamma+\Gamma\left(\frac{\omega^{3/2}}{\omega_\nu^{1/2}}\right)\right]^2}, \tag{4}$$

where $\omega_m=\Gamma/(1+\frac{2\pi\rho_{fluid}R^3}{3m})$ and $\omega_\nu=2\nu/R^2$. For systems incorporating inertia the usual definition of a corner frequency, $\omega_c=\kappa/\gamma_0$, clearly can no longer apply, so the dependence has been removed. The low density of air reduces the denominator of ω_m to close to unity, effectively removing any effective mass considerations as the entrained fluid is negligible [49]. Decomposing Eq. (3) into frequency components via Fourier theory [Eq. (31) in Berg-Sørensen and Flyvbjerg [41]] shows the larger kinematic viscosity of air, hence ω_ν, reduces any correction to Stokes' law compared to trapping in water.

The effect on the hydrodynamic correction of a negligible effective mass and larger ω_ν is not immediately apparent. To visualize the relative size of the correction we plot Fig. 1; the ratio of the power spectrum in Eq. (2) to the hydrodynamically correct version in Eq. (4).

Clearly for a given particle type and size the correction is significantly smaller when studying aerosols. However, the solid line shows the error begins to become significant for aerosols with a radius that would be considered relatively large for particles normally used in power spectrum-based studies in liquid. Should further studies be performed, the hydrodynamic correction must be investigated to improve accuracy and precision.

For the majority of applications, optical trapping parameters, such as trap stiffness, are only needed with an accuracy of ~10% and considering the magnitude of the correction factor we believe it is reasonable to neglect the effect of frequency-dependent friction in this study.

The second correction to be considered is that given by Faxén regarding the force on a sphere in motion near a plane surface, exactly what occurs when trapping with high numerical aperture (NA) optical tweezers due to the proximity of coverslips. Here we only consider the correction in the lateral direction although both axial and rotational equivalents exist [50,51]. Faxén's law shows the viscous drag on a sphere increases as it approaches a plane surface according to [52]

$$\Gamma_{Faxen}=\frac{\Gamma}{1-\left(\frac{9R}{16L}\right)+\frac{1}{8}\left(\frac{R}{L}\right)^3-\frac{45}{256}\left(\frac{R}{L}\right)^4-\frac{1}{16}\left(\frac{R}{L}\right)^5}, \tag{5}$$

where L is the distance between sphere center and surface. For the particle sizes studied here, this can have a dramatic effect on the friction experienced; even when trapping at distances approaching 40 μm from coverslips, there can be a 7% increase.

The final theoretical consideration is that in order to compare power spectra in given data sets we must calculate the detection system sensitivity, β, given in volts output per unit displacement of the particle. This is because the sensitivity can alter between experiments due to variations in power or simply geometry at the focus. Finding β allows voltage power spectra, those recorded directly from the experiment, to be converted to physical spectra, nm^2 Hz^{-1} versus Hz. Conventional methods rely on the relative simplicity of colloidal systems by using, for example, the drag force method [53], its extension to an oscillating sample stage [54] or moving a fixed bead over a known distance through the laser beam waist [55]. Clearly the former two would be difficult to implement in air and the latter is obviously not a good replica of experimental conditions [56]. A recent technique has been demonstrated that combines two methods to measure detector calibration from experimentally measured values alone [54]. It is hoped, even with the unique problems of airborne trapping, by using AODs or SLMs to oscillate the trap position, this technique will be developed for future experiments.

Here we are not concerned with high precision and for simplicity we calculate the detector sensitivity, β, from an uncalibrated voltage power spectrum $S^V(\omega)=\beta^2 S_{inert}(\omega)$ using the plateau value, P^V, reached for $\omega\gg\Omega$ in the function $\omega^4 S^V(\omega)$ [13]. We find the detector sensitivity, β, to be

$$\beta=\sqrt{\frac{P^V m}{2k_BT\Gamma}}. \tag{6}$$

III. EXPERIMENTAL

Droplets are trapped using a custom built inverted tweezers pictured in Fig. 2. The beam from a 532 nm Laser Quantum Finesse 4W c.w. laser is expanded by a Keplerian telescope to slightly overfill [57] the back aperture of a Nikon Plan 100x (NA=1.25 [58]) oil immersion microscope objective. The beam is focused though a type one cover slip into an aerosol chamber constructed from a cylindrical plastic enclosure 9 mm in height and 35 mm in diameter. This pro-

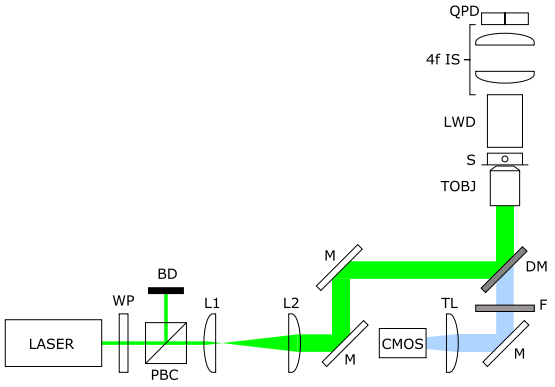

FIG. 2. (Color online) Apparatus diagram. A Gaussian beam is expanded by lenses L1 and L2 and directed to slightly overfill the back aperture of the Nikon objective (TOBJ) with mirrors M and DM. The long working distance objective (LWD) collects the scattered light from the droplet and its back aperture is imaged onto the QPD via a 4f lens system. Power is controlled using a polarizing beam cube (PBC) and half wave plate (WP). The same Nikon objective with an appropriate tube lens (TL) is used to image the sample (S) through a dichroic mirror (DM) and filter (F) onto the firewire camera (CMOS). The QPD, COBJ, and TOBJ are each mounted on three axis translation stages with the axial axis of TOBJ controlled either manually or by digital micrometer. BD is a beam dump.

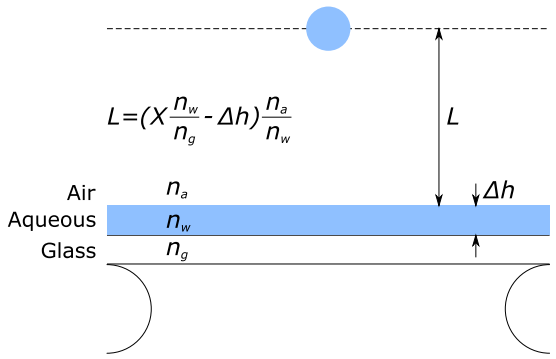

FIG. 3. (Color online) Enlarged view of the trapping region in the sample of Fig. 2. The refractive indices of the coverslip and index matched oil, water, and air are n_g, n_w, and n_a, respectively. Δh is the thickness of the water layer. Displacing the objective X microns from being focused on the first interface displaces the particle a distance L, given in the figure.

duces an enclosed environment where a high relative humidity can exist and also shields the trapping region from external air currents. The top of the chamber is made from a type zero cover slip to allow for transmission and then collection of the scattered trapping laser by a long working distance (LWD) Mitutoyo 100× (NA=0.55) objective, whose back aperture is imaged [11] equally onto the four quadrants of a quadrant photodiode (QPD) (Hamamatsu Silicon Diode Array S5980) via a 4f imaging system. The Mitutoyo objective also acts as the condenser lens for Köhler illumination (not shown). The Nikon objective and an appropriate tube lens images the sample through a laser filter onto a Basler A602f firewire camera.

The liquid aerosol is produced by nebulising a salt solution (20–80 g/L) with an Omron MicroAir NE-U22 vibrating mesh nebuliser which produces a polydisperse sample of liquid droplets with a mass median aerodynamic diameter of 4.9 μm [59]. The aerosol is transferred through a hole in the chamber side via a custom-made tapered glass nozzle [60].

The trapping beam is focused ~30 μm above the coverslips which are soaked in a 50% aqueous dilution of "Decon 90" for longer than one week. This treatment increases the hydrophilicity of the glass and once aerosol has been deposited on the cover slip, it provides a relatively thin, flat, and uniform film of water above which we trap. De-ionized water saturated tissue paper is also placed in the chamber to increase the relative humidity, but we ensure it does not touch the cover slip as this can induce flows in the water layer. Figure 3 shows an enlarged view of the trapping region geometry and also explains the relation between trapping height, L, and objective displacement, X.

Control over droplet size was required to fully investigate observed phenomena. First, this was achieved imprecisely by varying the concentration of the nebulised salt solution [45] as a higher concentration decreases the droplets vapor pressure allowing them to equilibrate with their surroundings at larger sizes. Second, more precise size selectivity can be induced with, on average, a positive linear dependence of captured droplet size on laser power [34,35].

Having trapped a droplet, the nebuliser is turned off. Once the droplet has reached equilibrium with its surrounding environment, and the remaining aerosol settled, the current produced by the detection of light on the QPD is sent, via shielded cables, to amplification electronics [61] containing a 50 kHz antialiasing filter. Data was acquired at a sampling frequency of 50 kHz for four seconds with a National Instruments PCI-6014E DAQ card, in differential mode. The voltage difference between left and right pairs of quadrants on the QPD represents the x position and the difference between the top and bottom pairs represents the y position. The voltage versus time data was Fourier transformed using LabVIEW and all remaining data analysis was performed offline at a later time. In order to minimize any parameter variation over time the experiments were carried out as quickly as possible with raw voltage versus time data not saved to increase speed still further. The detailed analysis of the data obtained for a colloidal case is extensively described in Berg-Sørensen and Flyvbjerg [41], and much remains the same here. An image of the trapped droplet was also taken with each power spectrum for later analysis.

To further reduce background noise, work was always carried out, where possible, solitarily in the laboratory with the laser used at >30% capacity and power control achieved by using a pair of half wave plates with polarizing beam cubes. The beam was first split for two different experiments and the second controlled power for this experiment alone. The power was varied between a minimum of 0.702 ± 0.009 mW and a maximum of 510 ± 6 mW.

Unlike tweezing in water, simply increasing the trapping power does not assist in capturing an aerosol droplet from the nebulised cloud and as such initial laser power must be carefully selected. Each droplet trapped was subjected to an increase in laser power in uniform steps with power spectra

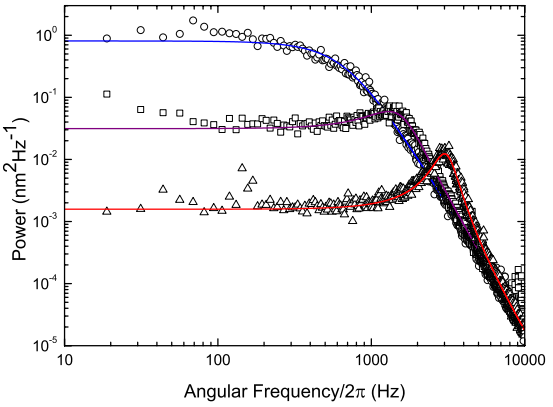

FIG. 4. (Color online) Power spectra of a droplet of radius 3.7 ± 0.2 μm trapped at powers 40.9 ± 0.5 (circles), 130 ± 2 (squares), and 356 ± 4 (triangles) mW resulting in damping ratios of 1.69 ± 0.04, 0.794 ± 0.01, and 0.364 ± 0.001, respectively. The fitting parameters for the top (blue), middle (purple) and bottom (red) curves are $\Omega/2\pi = 690 \pm 13$, 1565 ± 7, 3106 ± 13 Hz and $\Gamma/2\pi = 1167 \pm 13$, 1242 ± 17, 1131 ± 13 Hz, respectively. As the power increases, the appearance of a resonance peak is clear, indicating the move into an underdamped regime, along with a decrease in area and hence position variance. The natural frequency increases with laser power because of the associated increase in lateral trap stiffness, κ.

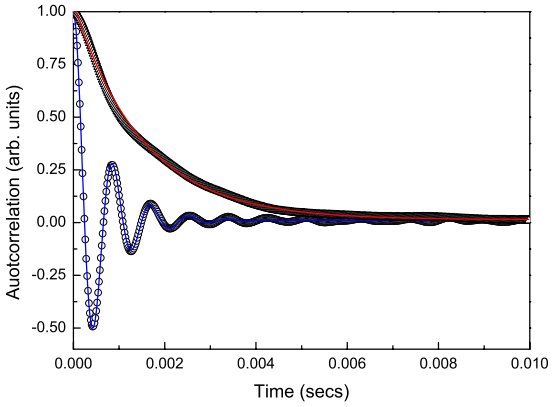

FIG. 5. (Color online) Plot of experimental autocorrelation data with associated fits for a 5.2 ± 0.2 μm optically trapped aerosol in an over-(triangles) and underdamped (circles) state trapped with powers 74 ± 1 and 442 ± 7 mW, respectively. Both traces clearly follow the classic exponential decay except in the underdamped case there is also the sinusoidal oscillation expected.

measurements taken at each. The minimum attainable damping ratio for each droplet was taken from the last power spectrum measured before it fell from the trap upon increasing the power (i.e., the highest power). This represents an upper limit on the ratio for that size.

To study how the water-air interface to droplet height may affect the dynamics we simply keep a constant laser power and vary the height of the sample stage, controlled and measured by a micrometer. The water layer thickness was measured by observing when a reflection of the trapping beam focus is obtained at both the water-air and glass-water interfaces. Having been focused through two refractive index mismatched interfaces (glass to water and water to air), there will be an associated focal shift [62] of which a rigorous description is complex [63,64] and not discussed here. A simple paraxial approximation is used to calculate the droplets position inside the chamber given a vertical displacement of the sample stage around a fixed objective. Modeling of the axial equilibrium position of the trap and experiments imaging the droplet from the side indicate that the relationship between droplet height and objective displacement is linear (data not shown) supporting the paraxial assumption [33,65].

IV. RESULTS AND ANALYSIS

Typical power spectra of position fluctuations from optically trapped droplets are shown in Fig. 4, illustrating, for a 3.7 ± 0.2 μm radius droplet, the ease with which the system can be transferred between over- and underdamped dynamics by varying laser power. The tail falls off with ω^{-4} as expected for $\omega \gg \Omega$ from Eq. (2) and a clear resonance peak begins to establish itself with increasing power, indicative of the droplet moving through the critical and into the underdamped regime.

For completeness, a plot of the autocorrelation function [16] of a single droplet in an under- and overdamped state is shown in Fig. 5. It shows the classic exponential decay for overdamped motion and sinusoidal oscillation enveloped by exponential decay for underdamped oscillators as expected.

The trend seen in Fig. 4 remains for all droplets; an increase in power increases lateral trap stiffness and moves the system toward or into the underdamped regime. A range of damping ratios has been observed from 3.57 ± 0.07 down to 0.260 ± 0.006 over the 4.7 ± 0.5 μm radius range studied. There is also an associated decrease in area under the power spectrum curve with increasing laser power, indicating a reduction in the position variance of the droplet.

The inclusion of inertial terms in the Brownian theory means only the mass of the particle is needed to calculate trap stiffness. Using the radius from video microscopy we obtain lateral trap stiffness values ranging from 0.12 ± 0.10 to 98 ± 17 pN μm^{-1} for 1.0 ± 0.3 to 5.7 ± 0.4 μm radius droplets.

One would expect the natural frequency of trapped droplets to vary as the square root of laser power, assuming the trap stiffness is linearly proportional to trapping power. This is confirmed in Fig. 6 for a 1.8 ± 0.2 μm radius droplet. For the range of radii and powers studied here we observe natural frequencies between $2\pi(328 \pm 12)$ rads^{-1} and $2\pi(3433 \pm 15)$ rads^{-1}. This range starts close to and ends well above the corner frequencies measured by tweezers in liquid based systems, although obviously not directly comparable.

The above results produce a downward shift in damping ratio by increasing lateral trap stiffness with larger laser powers. A decrease in friction felt by the droplet could likewise shift the ratio by varying the damping and as stated earlier Faxén's correction predicts that the proximity of a surface to our microscopic object heavily influences this. Exploiting this surface to droplet height dependence, Fig. 7 demon-

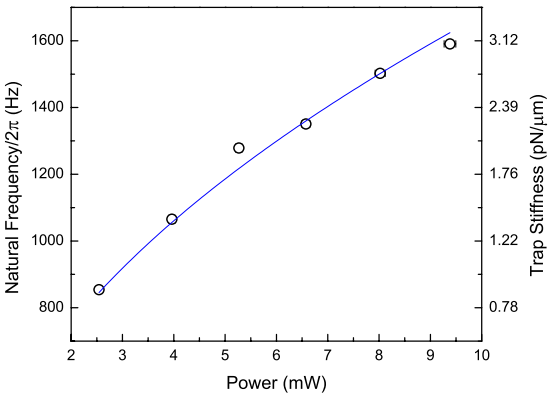

FIG. 6. (Color online) An example of how natural frequency for a 1.8 ± 0.2 μm radius droplet increases with the square root of laser power as expected from $\Omega = \sqrt{\kappa/m}$. The lateral trap stiffness axis is displayed for interest and is nonlinear. The error bars are standard error of the mean for the natural frequency rather than the trap stiffness (although they are smaller than the points themselves).

strates that lowering the sample stage, hence increasing the distance, reduces the damping and transfers the system from over- to underdamped. Note the resonance peak remains approximately at the same frequency for each spectrum as only the damping is changing, not the trap stiffness, contrary to Fig. 4.

Extracting damping values from data similar to Fig. 7, we can plot the dependence of friction upon droplet-surface height to obtain Fig. 8 [1]. Here the micrometer raised the sample stage in increments of 1 μm, decreasing to 0.5 μm as the surface was approached.

In Fig. 9 we plot the natural frequency as a function of height from the water layer. There is a steady fall-off with

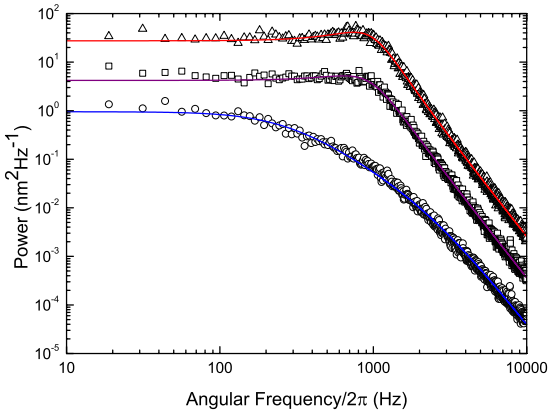

FIG. 7. (Color online) Power spectra demonstrating changes in damping as a function of surface-droplet distance for a 3.8 ± 0.2 μm radius droplet trapped with 46.3 ± 0.6 mW. The droplet was moved to heights of 4 ± 1 μm (circles), 9 ± 1 μm (squares), and 14 ± 1 μm (triangles) above the water layer resulting in damping ratios of 3.40 ± 0.06, 1.06 ± 0.01, and 0.92 ± 0.01, respectively. The fitting parameters for the top (red), middle (purple), and bottom (blue) curves are $\Omega/2\pi = 981 \pm 5$, 962 ± 5, 815 ± 10 Hz and $\Gamma/2\pi = 904 \pm 10$, 1019 ± 12, 2773 ± 32 Hz, respectively. The middle and top spectra are multiplied by 25 and 200 respectively to displace the data on the y axis for clarity.

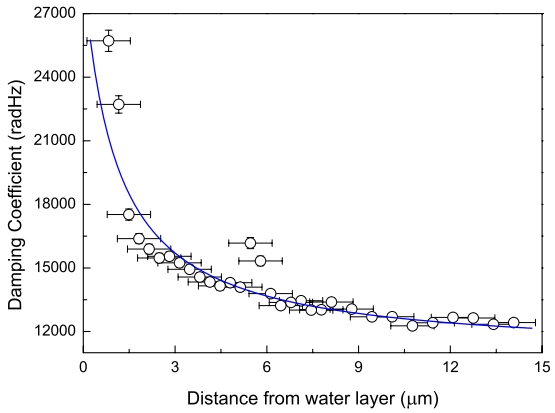

FIG. 8. (Color online) Variation of damping experienced by a droplet, trapped with 6.2 ± 0.1 mW, as a function of surface-droplet height [1]. The error bars are standard error of the mean.

distance indicating the spherical aberration induced is degrading the trap stiffness. Unlike the data of Vermeulen *et al.* [56] the data is approximately linear as the trap stiffness is independent of the viscous damping.

Figures 4–6 and 9 confirm the simple harmonic oscillator model applies to our experimental system for all regimes of damping. Our results are not precise enough to examine the need for frequency-dependent hydrodynamic correction, but Figs. 7 and 8 do show Faxén's correction has an important effect on the damping experienced.

Bearing this in mind, we turn to the most curious unusual phenomena observed; the loss of droplets from traps at a particular upper limit on laser power. The confirmation of a simple harmonic oscillator model as an appropriate description of our system leads us to test the hypothesis that the particles become largely underdamped so quickly that instability is caused. To test this and ascertain the true cause, we plot in Fig. 10 the upper limit on the minimum damping ratio attainable against droplet radius.

Figure 10 illustrates droplets can exist in an underdamped regime. Some droplets are lost from traps while overdamped and some while underdamped. This suggests no instability is induced as the object crosses the critical damping point and

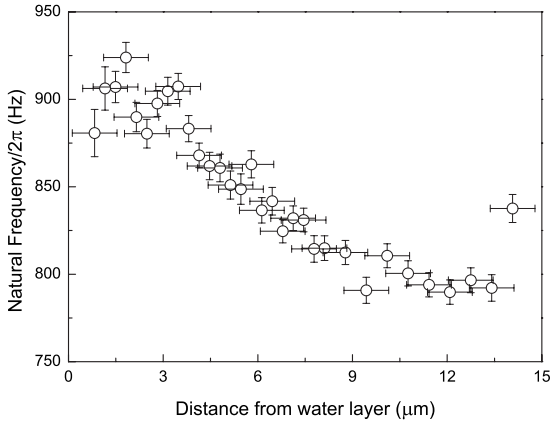

FIG. 9. Natural frequency as a function of distance from water layer for the droplet in Fig. 7. The error bars are standard error of the mean.

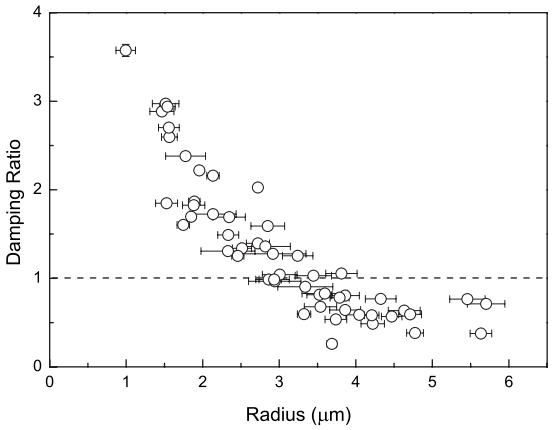

FIG. 10. Upper limit on the minimum attainable damping ratio against droplet radius. It is an upper limit as we increase the laser power in finite increments. The dashed horizontal line represents a critically damped system. The error bars are standard error of the mean.

so is not the reason for droplet loss with increasing trapping power. There is a clear size dependence but one must be careful to note this does not lead to the conclusion that droplets do indeed become unstable as they reach a particular damping threshold, but rather fall from the optical traps at a certain upper limit on trapping power.

V. DISCUSSION

The reader may notice significantly more scatter in the results of this investigation compared to experiments using similar techniques in liquid. The reasons will now be discussed briefly showing the complex nature of the experiment and the engineering challenges faced to improve future precision.

The majority of previous work using the power spectrum method is based on tweezing solid microspheres, with precisely known radii, in the liquid phase allowing very high precision studies; indeed, the ability to detect sphere nonuniformity is possible [54]. In the studies here a large source of error is measuring the radius using video microscopy with the likely errors propagating heavily into some of the systems calculated properties ($\kappa \propto m \propto R^3$). Trapping of solid aerosols with known radii would remove this problem, but this is more difficult [60]. In addition, highly precise radius measurements are possible via cavity enhanced Raman scattering (CERS) [66] but require sensitive spectrometers. We have shown in a previous publication that fitting to the data of Fig. 8 with Eq. (5) allows the droplet radius to be measured with good precision [1].

It is difficult to determine which individual factor, trap stiffness, or damping, contributes to the variation in damping ratio for any given experiment. For an individual droplet, the surrounding conditions can remain relatively constant over the time of a single experiment as, with no additional aerosol flow from the nebuliser, the droplet quickly reaches equilibrium with its surroundings. To trap another droplet, nebulisation must resume where upon the chamber conditions can alter. Additional aerosol can settle on the coverslip changing the thickness of the aqueous layer and hence the optical potential [64,65,67] at the trap site together with the proximity of the particle to the surface [41,52,65]. As mentioned, variation in trapping power between droplets alters the height of the droplet [33] and hence distance from the underlying water layer, thus again altering the optical potential and damping. These factors contribute to the rather complex and difficult analysis of the system.

The difficult nature, relative to colloidal tweezers, of trapping in air imposes several important experimental methods. A long working distance condenser must be used due to the aerosol chamber height, but a higher NA lens may have been desirable to improve detector sensitivity [68]. Most colloidal experiments use monodisperse suspensions of solid particles thus allowing an arbitrary number of measurement repetitions; often up to 100 power spectra are averaged. However, aerosol droplets are continuously finding an equilibrium with the surrounding environment, so the conditions of the experiment may not remain constant long enough for repeated measurements to improve precision, hence the choice of sampling and no averaging over multiple power spectra. Also, we are looking at an inherently unstable region with the aim, at times, of losing the trapped droplet so, clearly, another particle of the exact same size and composition cannot be found. With the current iteration of apparatus, there is a clear trade off between speed and precision.

Some studies have used a secondary, independent probe beam to monitor position fluctuations as this allows greater flexibility and perhaps improved accuracy [69]. We employ only a single beam because a very small amount of power is needed to tweeze in air [35] and a second beam has the potential to significantly alter the optical potential at the trap site.

In future studies we suggest that a system including a 'science chamber' be developed where many variables can be controlled. A particle could be trapped and transferred to such a chamber with relative humidity control, with or without a water layer, and with a lower physical profile to enable the use of higher NA condenser optics. Also, as the mechanical stability of our system is not yet fully optimized, the precision could be improved.

Not discussed in detail here is that Faxén derived his correction for a sphere moving with constant velocity, which is not the case. Therefore the frequency-dependent friction should be combined with Faxén's correction for a complete solution [41,54]. Also, when dealing with solid in fluid systems no slipping occurs at the boundary between the two materials upon translation. However, the physics involved becomes more complicated when studying fluid in fluid systems; slip can occur. Due to the possibility of slip at the surface of the fluid sphere, flow can be induced inside the water droplet. This flow causes reduction of the well known prefactor of Stokes' law [52,70] according to

$$F_{stokes} = -\frac{6\pi\nu\rho_{fluid}Rv}{C_c}\frac{1+\frac{2}{3}\sigma}{1+\sigma}, \tag{7}$$

where σ is the ratio of the dynamic viscosities of the medium and droplet. Hence Stokes' law for a water droplet in air is given by

$$F_{stokes} = -\frac{5.96\pi\nu\rho R v}{C_c}, \tag{8}$$

which has been taken into account in the data analysis here.

VI. CONCLUSION

The work here is the first parameter exploration of the Brownian motion of optically trapped liquid aerosols. We have presented evidence that the system is suitably described by a simple harmonic oscillator model, which must include a description of Faxén's correction, but not necessarily frequency-dependent hydrodynamic corrections to Stokes' law. The results also show there is difficulty in decoupling the parameters responsible for the observed behavior. Having hypothesized that an instability is caused in the system when crossing from over- to underdamped regimes, we see this is not supported by the evidence.

Considering the Langevin equation it is seen that there are only four processes providing forces that give rise to droplet position fluctuations, namely Brownian white noise, friction, inertia, and the optical force. Having rejected any damping or inertial cause for the instabilities with the evidence presented here, the logical conclusion is that the optical force must determine whether the droplet remains trapped or not and gives rise to the size dependence of Fig. 10. This will be discussed in a further publication.

The investigation has provided results extending the boundaries of precise studies of Brownian motion in optical tweezers into a new damping regime. It is hoped these results will provide researchers with a new understanding of optical tweezers for studies in both fundamental and applied science, providing a rich playground of study in the underdamped regime.

ACKNOWLEDGMENTS

We thank EPSRC for funding this work. DRB would like to thank EPSRC and the Lindemann Trust for support. D.M. thanks the Royal Society.

[1] D. R. Burnham and D. McGloin, New J. Phys. **11**, 063022 (2009).
[2] R. Di Leonardo, G. Ruocco, J. Leach, M. J. Padgett, A. J. Wright, J. M. Girkin, D. R. Burnham, and D. McGloin, Phys. Rev. Lett. **99**, 010601 (2007).
[3] D. McGloin, D. R. Burnham, M. D. Summers, D. Rudd, N. Dewar, and S. Anand, Faraday Discuss. **137**, 335 (2008).
[4] K. Berg-Sorensen and H. Flyvbjerg, New J. Phys. **7**, 38 (2005).
[5] A. Einstein, *Investigations on the Theory of the Brownian Movement* (Dover Publications, New York, 1956).
[6] Z. G. Sun, C. D. Tomlin, and E. M. Sevick-Muraca, Langmuir **17**, 6142 (2001).
[7] S. Sudol, Y. Miyasaka, and K. Otsukam, Opt. Express **14**, 1044 (2006).
[8] R. Newburgh, J. Peidleb, and W. Ruecknerc, Am. J. Phys. **74**, 478 (2006).
[9] M. J. Lang, C. L. Asbury, J. W. Shaevitz, and S. M. Block, Biophys. J. **83**, 491 (2002).
[10] G. Pesce, A. Sasso, and S. Fusco, Rev. Sci. Instrum. **76**, 115105 (2005).
[11] A. Rohrbach, C. Tischer, D. Neumayer, E. Florin, and E. H. K. Stelzer, Rev. Sci. Instrum. **75**, 2197 (2004).
[12] C. Hertlein, L. Helden, A. Gambassi, S. Dietrich, and C. Bechinger, Nature (London) **451**, 172 (2008).
[13] M. W. Allersma, F. Gittes, M. J. deCastro, R. J. Stewart, and C. F. Schmidt, Biophys. J. **74**, 1074 (1998).
[14] W. Denk and W. W. Webb, Appl. Opt. **29**, 2382 (1990).
[15] L. Ghislain, N. Switz, and W. Webb, Rev. Sci. Instrum. **65**, 2762 (1994).
[16] J. C. Meiners and S. R. Quake, Phys. Rev. Lett. **82**, 2211 (1999).
[17] Y. Deng, J. Bechhoefer, and N. R. Forde, J. Opt. A, Pure Appl. Opt. **9**, S256 (2007).
[18] L. I. McCann, M. Dykman, and B. Golding, Nature (London) **402**, 785 (1999).
[19] D. M. Carberry, M. A. B. Baker, G. M. Wang, E. M. Sevick, and D. J. Evans, J. Opt. A, Pure Appl. Opt. **9**, S204 (2007).
[20] A. Pertsinidis and X. S. Ling, Phys. Rev. Lett. **87**, 098303 (2001).
[21] M. Polin, D. G. Grier, and S. Quake, Phys. Rev. Lett. **96**, 088101 (2006).
[22] S. Lee and D. G. Grier, J. Phys.: Condens. Matter **17**, S3685 (2005).
[23] A. Chowdhury, B. J. Ackerson, and N. A. Clark, Phys. Rev. Lett. **55**, 833 (1985).
[24] J. Joykutty, V. Mathur, V. Venkataraman, and V. Natarajan, Phys. Rev. Lett. **95**, 193902 (2005).
[25] L. Pedersen and H. Flyvbjerg, Phys. Rev. Lett. **98**, 189801 (2007).
[26] A. M. Yao, S. A. J. Keen, D. R. Burnham, J. Leach, R. Di Leonardo, D. McGloin, and M. J. Padgett, New J. Phys. **11**, 053007 (2009).
[27] A. Ashkin and J. M. Dziedzic, Appl. Phys. Lett. **19**, 283 (1971).
[28] L. Mitchem and J. P. Reid, Chem. Soc. Rev. **37**, 756 (2008).
[29] M. Guillon, R. E. H. Miles, J. P. Reid, and D. McGloin, New J. Phys. **11**, 103041 (2009).
[30] J. R. Butler, L. Mitchem, K. L. Hanford, L. Treuel, and J. P. Reid, Faraday Discuss. **137**, 351 (2008).
[31] M. D. King, K. C. Thompson, and A. D. Ward, J. Am. Chem. Soc. **126**, 16710 (2004).
[32] T. Li, S. Kheifets, D. Medellin, and M. G. Raizen, Science **328**, 1673 (2010).
[33] K. J. Knox, J. P. Reid, K. L. Hanford, A. J. Hudson, and L. Mitchem, J. Opt. A, Pure Appl. Opt. **9**, S180 (2007).
[34] R. J. Hopkins, L. Mitchem, A. D. Ward, and J. P. Reid, Phys. Chem. Chem. Phys. **6**, 4924 (2004).
[35] D. R. Burnham and D. McGloin, Opt. Express **14**, 4175 (2006).

[36] K. C. Neuman and S. M. Block, Rev. Sci. Instrum. **75**, 2787 (2004).
[37] J. C. Crocker and D. G. Grier, J. Colloid Interface Sci. **179**, 298 (1996).
[38] J. H. G. Huisstede, K. O. van der Werf, M. L. Bennink, and V. Subramaniam, Opt. Express **13**, 1113 (2005).
[39] G. Volpe, G. Volpe, and D. Petrov, Phys. Rev. E **76**, 061118 (2007).
[40] L. D. Landau and E. M. Lifshitz, *Fluid Mechanics* (Pergamon Press, New York, 1959).
[41] K. Berg-Sørensen and H. Flyvbjerg, Rev. Sci. Instrum. **75**, 594 (2004).
[42] M. C. Wang and G. E. Uhlenbeck, Rev. Mod. Phys. **17**, 323 (1945).
[43] S. Chandrasekhar, Rev. Mod. Phys. **15**, 1 (1943).
[44] H. Risken, *The Fokker-Plank Equation: Methods of Solution and Applications*, 2nd ed. (Springer, New York, 1989).
[45] J. H. Seinfeld and S. N. Pandis, *Atmospheric Chemistry and Physics: From Air Pollution to Climate Change* (Wiley-Interscience, New York, 1997).
[46] G. G. Stokes, Trans. Cambridge Philos. Soc. **IX**, 8 (1850).
[47] S. Keen, J. Leach, G. Gibson, and M. J. Padgett, J. Opt. A, Pure Appl. Opt. **9**, S264 (2007).
[48] M. Li and J. Arlt, Opt. Commun. **281**, 135 (2008).
[49] A. Widom, Phys. Rev. A **3**, 1394 (1971).
[50] E. Schaffer, S. F. Norrelykke, and J. Howard, Langmuir **23**, 3654 (2007).
[51] J. Leach, H. Mushfique, S. Keen, R. Di Leonardo, G. Ruocco, J. M. Cooper, and M. J. Padgett, Phys. Rev. E **79**, 026301 (2009).
[52] J. Happel and H. Brenner, *Low Reynolds Number Hydrodynamics: With Special Applications to Particulate Media* (Prentice-Hall, Englewood Cliffs, NJ, 1965).
[53] N. Malagnino, G. Pesce, A. Sasso, and E. Arimondo, Opt. Commun. **214**, 15 (2002).
[54] S. F. Tolic-Nørrelykke, E. Schäffer, J. Howard, F. S. Pavone, F. Juelicher, and H. Flyvbjerg, Rev. Sci. Instrum. **77**, 103101 (2006).
[55] A. Pralle, M. Prummer, E. L. Florin, E. H. K. Stelzer, and J. K. H. Hörber, Microsc. Res. Tech. **44**, 378 (1999).
[56] K. Vermeulen, G. Wuite, G. Stienen, and C. Schmidt, Appl. Opt. **45**, 1812 (2006).
[57] A. Ashkin, Biophys. J. **61**, 569 (1992).
[58] It is important to note that the NA can clearly not be larger than unity in the focal region and in fact due to total internal reflection at the glass:water:air boundary the NA is effectively reduced to ~0.67.
[59] Datasheet accompanying Omron MicroAir NE-U22 nebuliser.
[60] M. D. Summers, D. R. Burnham, and D. McGloin, Opt. Express **16**, 7739 (2008).
[61] F. Pampaloni, *Force Sensing and Surface Analysis with Optically Trapped Microprobes* (Universität Regensburg, Regensbury, 2002).
[62] K. C. Neuman, E. A. Abbondanzieri, and S. M. Block, Opt. Lett. **30**, 1318 (2005).
[63] P. Török, P. Varga, Z. Laczik, and G. R. Brooker, J. Opt. Soc. Am. A **12**, 325 (1995).
[64] P. Török and P. Varga, Appl. Opt. **36**, 2305 (1997).
[65] D. R. Burnham and D. McGloin (unpublished).
[66] L. Mitchem, J. Buajarern, R. J. Hopkins, A. D. Ward, R. J. J. Gilham, R. L. Johnston, and J. P. Reid, J. Phys. Chem. A **110**, 8116 (2006).
[67] N. B. Viana, M. S. Rocha, O. N. Mesquita, A. Mazolli, P. A. Maia Neto, and H. M. Nussenzveig, Phys. Rev. E **75**, 021914 (2007).
[68] A. Rohrbach, H. Kress, and E. H. K. Stelzer, Opt. Lett. **28**, 411 (2003).
[69] E. Fällman, S. Schedin, J. Jass, M. Andersson, B. E. Uhlin, and O. Axner, Biosens. Bioelectron. **19**, 1429 (2004).
[70] H. Lamb, *Hydrodynamics*, 6th ed. (Cambridge University Press, Cambridge, England, 1932).